

See discussions, stats, and author profiles for this publication at: <https://www.researchgate.net/publication/262844050>

Detailed Microscopic Unfolding Pathways of an α -Helix and a β -Hairpin: Direct Observation and Molecular Dynamics

ARTICLE in THE JOURNAL OF PHYSICAL CHEMISTRY B · JUNE 2014

Impact Factor: 3.3 · DOI: 10.1021/jp500955z · Source: PubMed

CITATIONS

4

READS

59

5 AUTHORS, INCLUDING:



Gouri S. Jas

Central University of the Caribbean

44 PUBLICATIONS 1,826 CITATIONS

[SEE PROFILE](#)



Wendy Hegefledt

Scott & White

6 PUBLICATIONS 78 CITATIONS

[SEE PROFILE](#)



Charles Russell Middaugh

University of Kansas

371 PUBLICATIONS 9,282 CITATIONS

[SEE PROFILE](#)



Krzysztof Kuczera

University of Kansas

116 PUBLICATIONS 14,350 CITATIONS

[SEE PROFILE](#)

Detailed Microscopic Unfolding Pathways of an α -Helix and a β -Hairpin: Direct Observation and Molecular Dynamics

Gouri S. Jas,^{*,†} Wendy A. Hegefled,^{||} C. Russell Middaugh,[†] Carey K. Johnson,[‡] and Krzysztof Kuczera^{*,‡,§}

[†]Department of Pharmaceutical Chemistry, University of Kansas, Lawrence, Kansas 66047, United States

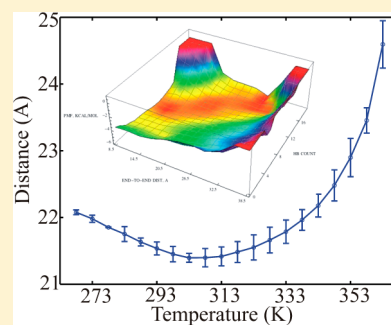
[‡]Department of Chemistry, University of Kansas, Lawrence, Kansas 66045, United States

[§]Department of Molecular Biosciences, University of Kansas, Lawrence, Kansas 66045, United States

^{||}Department of Chemistry, Biochemistry, and Institute of Biomedical Studies, Baylor University, Waco, Texas 76706, United States

Supporting Information

ABSTRACT: We present a combined experimental and computational study of unfolding pathways of a model 21-residue α -helical heteropeptide (W_1H_5 -21) and a 16-residue β -hairpin (GB41–56). Experimentally, we measured fluorescence energy transfer efficiency as a function of temperature, employing natural tryptophans as donors and dansylated lysines as acceptors. Secondary structural analysis was performed with circular dichroism and Fourier transform infrared spectroscopy. Our studies present markedly different unfolding pathways of the two elementary secondary structural elements. During thermal denaturation, the helical peptide exhibits an initial decrease in length, followed by an increase, while the hairpin undergoes a systematic increase in length. In the complementary computational part of the project, we performed microsecond length replica-exchange molecular dynamics simulations of the peptides in explicit solvent, yielding a detailed microscopic picture of the unfolding processes. For the α -helical peptide, we found a large heterogeneous population of intermediates that are primarily frayed single helices or helix-turn-helix motifs. Unfolding starts at the termini and proceeds through a stable helical region in the interior of the peptide but shifted off-center toward the C-terminus. The simulations explain the experimentally observed non-monotonic variation of helix length with temperature as due primarily to the presence of frayed-end single-helix intermediate structures. For the β -hairpin peptide, our simulations indicate that folding is initiated at the turn, followed by formation of the hairpin in zipper-like fashion, with $C\alpha \cdots C\alpha$ contacts propagating from the turn to termini and hairpin hydrogen bonds forming in parallel with these contacts. In the early stages of hairpin formation, the hydrophobic side-chain contacts are only partly populated. Intermediate structures with low numbers of β -hairpin hydrogen bonds have very low populations. This is in accord with the “broken zipper” model of Scheraga. The monotonic increase in length with temperature may be explained by the zipper-like breaking of the hairpin hydrogen bonds and backbone contacts.



INTRODUCTION

The formation of secondary structures, α -helices, and β -strands is one of the most fundamental processes along the folding trajectory of a protein. However, detailed information on the pathways of formation of helix and sheet remains unclear. A microscopic detailed picture would be highly useful to both our knowledge of peptide structure and dynamics and a fundamental understanding of protein folding. Possible insights into the various diseases caused by protein misfolding such as Alzheimer’s disease, Parkinson’s disease, and Huntington’s disease make the protein folding problem also an important area of biomedical research.¹

To uncover microscopic details of the unfolding pathway of the two very important secondary structural elements, we undertook an investigation of the model peptides, Ac-WAAAH⁺-(AAARA)₃A-NH₂ (W_1H_5 -21) representing an α -helix and GEWTYDDATKTFTVTE (GB41–56) representing a β -hairpin. These peptides are large enough to form well-

defined stable three-dimensional structures in solution while being more amenable to spectroscopic and modeling studies than more complex protein systems. We employed a joint experimental and computational approach. Experimentally, we used Förster resonance energy transfer (FRET)² to provide new information on the changes in the conformational distributions along the folding pathway. Computationally, we performed a detailed analysis of the sampled structures using replica-exchange molecular dynamics (REMD), which permits a complete conformational sampling of the studied systems. Compared to previous studies, our simulations have several novel features, involving a significant increase in length in the 1 μ s/replica range, use of updated versions of force fields, and inclusion of more solvent. Besides the standard measures of

Received: January 27, 2014

Revised: June 3, 2014

Published: June 4, 2014



folding, we also calculate the predicted effect of unfolding on the FRET efficiency and present a novel analysis of the conformational landscape. Ultimately, we wanted to use the new experimental and simulation data to provide new details of folding pathways of both helices and sheets.

The W₁H₅-21 helix-forming peptide has been the subject of several previous experimental investigations. Temperature jump kinetics measurements were used to determine a 300 ns relaxation time for this system at 301 K³ and a fractional-power dependence of the rate of helix formation on viscosity.⁴ Circular dichroism (CD) was used to determine the melting curve of this peptide, predicting a fractional helix population of about 50% at 296 K.⁵ For a related system, isotopic labeling and resonance Raman spectroscopy were used to show that the central part of a 21-residue peptide formed a more stable helical structure than the ends.⁶ Related to our study, small-angle X-ray scattering for a series of helix-forming peptides demonstrated that the radii of gyration tended to be shorter than those expected for ideal helices, a result that was interpreted in terms of a “broken helix” model.⁷ More recently, structure and kinetics information has emerged for relatively small helix-forming peptides. Relaxations of ca. 5 ns and ca. 1 ns were measured for the blocked pentapeptide Ac-WAAAH⁺-NH₂ (WHS),⁸ while the presence of helical structure was confirmed by NMR and CD spectroscopy.⁹ The presence of a low but measurable population of helical structure was also detected for a blocked pentaalanine peptide.¹⁰ Initial progress in analyzing residue specificity of helix folding includes finding a higher melting temperature in the center of the helix compared to the termini,⁶ relatively small variations in relaxation times along the chain in an unconstrained system,¹¹ and observation of larger variations of relaxation times with position in a constrained helix.¹²

For the GB41–56 (GB1) peptide, the formation of a hairpin structure was initially determined by NMR.¹³ Kinetic measurements yielded a relaxation time of 6 μ s at room temperature, which was interpreted in terms of a zipper model.¹⁴ GB1 and related peptides have been studied by a range of experimental methods, including IR, NMR, CD, and calorimetry,¹⁵ with a recent review of results presented elsewhere.¹⁶ The same work also discusses the different models of hairpin formation, and suggests that the available experimental data tend to support the broken zipper mechanism.¹⁶ The importance of the turn for hairpin initiation has been recognized.¹⁷

The folding of α -helices and β -hairpins has been the subject of numerous computational studies. Early work involving elevated temperatures or constraints found individual hydrogen bond breaking events on 10–100 ps time scales.¹⁸ Extensive simulations using implicit solvent models suggested either two-state¹⁹ or multistate folding²⁰ for model helices. Further progress was obtained by replica-exchange simulations, which generated helix melting curves,²¹ and showed that terminal residues exhibited lower folded populations than central sites and that shielding by side-chain atoms led to stabilization of neighboring backbone hydrogen bonds.²² Extensive studies of helices were carried out by Sorin and Pande, who used a distributed computing approach.²³ These authors found that helix folding is initiated at multiple nucleation sites, followed by extension of several helix fragments and their merging into a single helix. Helix formation has also been explored by direct MD for very short model peptides^{10,24} and by path exploration methods for larger systems.²⁵ Recently, we have presented analysis of the folding pathways of several alanine-based

peptides, including WHS and WH21 based on extensive REMD simulations.²⁶ For pentapeptide systems, the predicted folding paths tended to exhibit a dependence on force field. However, for WH21, the folding path was essentially the same with AMBER03, CHARMM27, and OPLS-AA models and showed folding proceeding first through an off-center region and then expanding to termini, with primarily single-helix and helix-turn-helix intermediates.²⁶

The GB1 peptide folding mechanism has also been the subject of numerous computational studies, starting with statistic-mechanical, coarse-grained, and implicit solvent approaches,^{14,27} replica-exchange,²⁸ and specialized molecular dynamics simulations.²⁹ A review of earlier studies may be found elsewhere.³⁰ The simulations have suggested three main mechanisms for GB1 hairpin folding: hydrophobic collapse, in which the compact structure with a native hydrophobic core forms before the interstrand hydrogen bonds, the zipper, in which folding starts at the central turn, followed by formation of the hairpin hydrogen bonds and finally the hydrophobic contacts and broken zipper pathway, in which the establishment of the turn is followed by formation of loose hydrophobic contacts and finally formation of hairpin hydrogen bonds and a native hydrophobic core.¹⁶ A fourth mechanism is reptation, in which folding is initiated by out-of-register interstrand hydrogen bonding, has also been proposed.³¹ Recently extensive folding simulations of hairpins have been performed, uncovering the presence of specific folding intermediates and nonexponential kinetics.³²

Our combined approach of FRET measurements and molecular modeling for carefully selected model peptide systems is aimed at providing new experimental information about the folding paths of helices and hairpins and proposing microscopic explanations for the observed effects, shedding new light on the mechanism of the formation of the basic units of secondary structure and on the protein folding problem in general.

METHODS

Model Peptides. Our α -helix model, Ac-WAAAH⁺-(AAARA)₃A-NH₂ (W₁H₅-21), has been designed with a high alanine content for helical propensity,³³ three arginines for improved solubility, and Trp1 and His5 for intrinsic monitoring of conformational change.³ To enhance Trp–His interaction, experiments are carried out under acidic conditions, where the His ring is protonated.³⁴ The Trp1 residue is also employed as the donor in FRET experiments. Our β -hairpin model is the peptide GEWTYDDATKTFTVTE (GB1), built from residues 41–56 of the second hairpin of the Ig-binding domain of streptococcal protein G.³⁵ This model system also includes a single tryptophan, Trp3, buried in a hydrophobic cluster. This residue can be utilized as a probe to monitor the unfolding reaction and as the donor in FRET experiments.^{3,34} The dansylated lysine acceptor is attached at the C-termini of both peptides. Thus, the donor–acceptor distance measured in our FRET experiments should be representative of the peptide end-to-end distance in both cases.

Materials. The 21-residue helical peptide Ac-WAAAH⁺-(AAAR⁺A)₃A-NH₂ (W₁H₅-21) and its dansylated form, Ac-WAAAH⁺-(AAAR⁺A)₃AK-(dansyl)-NH₂ (dan-W₁H₅-21), were purchased from GenScript Corporation (Piscataway, NJ, USA) and were >98% pure. The 16-residue β -hairpin peptide, GEWTYDDATKTFTVTE (GB1), and its dansylated form, GEWTYDDATKTFTVTEK-(dansyl-Lys), were purchased

from GenScript Corporation (Piscataway, NJ, USA) and were >98% pure. For all experiments, the W₁-H₅-21 peptides were dissolved in 20 mM acetate buffer, pH 4.8. The β -hairpin peptides were dissolved in 20 mM phosphate buffer, pH 7.2. Peptide concentrations were determined from the absorbance of tryptophan at 280 nm using an extinction coefficient of 5690 M⁻¹ cm⁻¹. In FRET, the energy transfer efficiency depends sharply on the distance between the acceptor and donor dyes roughly in a range within a factor of 2 of the Förster radius R_0 , the distance at which the FRET efficiency is 50%. For the donor–acceptor pair chosen for our studies, Trp and dansyl, the Förster radius is 21 Å, which covers the range of conformations of interest for our helical and hairpin systems.³⁶

■ EXPERIMENTS

Circular Dichroism. Temperature dependent far UV circular dichroism measurements of the dansylated and non-dansylated forms of the peptides were performed with a JASCO 815 spectropolarimeter (Tokyo, Japan) using a 0.5 mm path length cylindrical cell and concentrations of ~275 μM. Spectra were measured over 170–260 nm in the 266–363 K temperature range, in roughly 10 K increments. For melting curves, the wavelength was fixed to 222 nm for the W₁-H₅-21 peptides and to 201 nm for the β -hairpin peptides. An estimate of the thermodynamic properties and fractional helix population as a function of temperature were obtained by fitting melting curves from far UV CD with a two-state equilibrium model using the EXAM program.³⁷ The fitting procedure yielded temperature-independent values of the transition enthalpy ΔH° and entropy ΔS° , and the melting temperature $T_m = \Delta H^\circ/\Delta S^\circ$. The Gibbs free energy was calculated as $\Delta G^\circ = \Delta H^\circ - T\Delta S^\circ$, and the equilibrium constant K was found through $\Delta G^\circ = -RT \ln(K)$. On the basis of a conservative estimate, the errors in the thermodynamic parameters were about 5%, similar to previous analyses.^{3–5} Singular value decomposition (SVD) was applied to the 170–260 nm CD scans to resolve overlapping spectral components.

Fourier Transform Infrared Spectroscopy. FTIR measurements were performed at 298 K with ~700 μM of the dansylated and non-dansylated helical and β -hairpin peptides. The samples were measured with CaF₂ windows with a 15 μm Teflon spacer to obtain a high resolution spectrum in the amide I band region. A total of 5000 scans were collected at a resolution of 1 cm⁻¹ in the spectral range 400–4000 cm⁻¹ using a Thermo Nicolet Nexus 670 FT-IR equipped with a XT-KBr beamsplitter and DTGS KBr detector. The contribution from the buffer solution was subtracted using OMNIC software (Thermo Electron Corporation). Data analysis was also performed with OMNIC utilizing Fourier self-deconvolution (FSD) and curve fitting procedures using least-squares fits with Gaussian profiles.

Fluorescence Spectroscopy. Measurements were made on a Horiba Jobin Yvon Fluorolog (Edison, NJ, USA) to monitor the intrinsic fluorescence of the Trp residue in the non-dansylated peptides and in the dansylated peptides undergoing FRET from Trp to dansyl. The samples were excited at 280 nm, and the emission spectra were recorded from 285 to 525 nm for non-dansylated and from 285 to 800 nm for dansylated peptides.³⁶ For all experiments, the temperature was measured every 5° from 268 to 363 K with a slit bandwidth of 2 nm and an integration time of 1.0 s. The same conditions were used for recording buffer scans, which were then subtracted from the appropriate peptide spectra.

Calculation of Donor–Acceptor Apparent Distance. The experimental data were analyzed using the Förster equation, which relates the energy transfer efficiency between the donor and acceptor (E) to the distance (r) between a donor (D) and acceptor (A):

$$r = R_0 [(1/E) - 1]^{1/6} \quad (1)$$

where R_0 is the Förster radius at which the transfer efficiency is 50% for a particular donor–acceptor pair. The Förster radius was calculated through

$$R_0 = (J\kappa^2 Q_0 n^{-4})^{1/6} \times 9.7 \times 10^3 \quad (2)$$

where J is the spectral overlap integral between the donor and acceptor, κ^2 reflects the relative orientation of the donor and acceptor transition dipoles, n is the refractive index of the medium between the donor and acceptor, and Q_0 is the quantum yield of the energy donor in the absence of an acceptor.^{2,36} The Förster radius is found to be 21 Å for the Trp and dansyl pair. The value for κ^2 was assumed to be 2/3, since the flexibility of the peptides and side chains should produce a relatively random orientation. The energy transfer efficiency was derived from

$$E = 1 - F_{DA}/F_D \quad (3)$$

where F_{DA} is the fluorescence intensity of the donor in the presence of the acceptor and F_D is the fluorescence intensity of the donor in the absence of an acceptor.³⁸ F_{DA} and F_D were taken from the integration of the fluorescence intensity between 310 and 440 nm.

Simulations of W₁H₅-21 Peptide. The starting point was a model α -helix structure built with CHARMM³⁹ with an acetylated N-terminus and amidated C-terminus and with His-5 in its protonated form, corresponding to acidic pH conditions. Further simulations were performed using GROMACS 4.0.4.⁴⁰ The system was solvated in a box of 3587 TIP3P⁴¹ waters, with 8 Na⁺ and 12 Cl⁻ ions added to neutralize the system and provide a physiological ionic strength. The AMBER03⁴² force field was used, with an 8.0 Å nonbonded cutoff and particle-mesh Ewald treatment of long-range electrostatics. The system was prepared by brief energy minimization, 50 ps of NVT molecular dynamics with positional restraints on the peptide at 300 K and 100 ps unrestrained NPT MD at 300 K and 1 bar, after which the final size of the cubic solvent box was 48.2 Å. The final structure was used to start a 1000 ns constant volume replica-exchange MD simulation. Fifty replicas with temperatures in the 290–500 K range were employed with exchange attempts every 1 ps and average acceptance ratios in the 0.19–0.36 range. The REMD simulations were carried out with constraints on all bonds, with an integration time step of 2 fs. The trajectory generation rate was about 20 ns per day running on 8 cores/replica on the Kodiak cluster at Baylor University.

Simulations of GB1 Peptide. The starting point was the β -hairpin structure for residues 41–56 from model 1 of PDB structure 1GB1, with standard charged termini. Simulations were performed using GROMACS 4.5.3.⁴⁰ The system was solvated in a box of 2941 TIP3P⁴¹ waters, with 9 Na⁺ and 6 Cl⁻ ions added to neutralize the system and provide a physiological ionic strength. The CHARMM version 27 protein force field³⁹ was used with a 13.0 Å nonbonded cutoff, switching of van der Waals interactions over 12–13 Å, and particle-mesh Ewald treatment of long-range electrostatics. The system was prepared by brief energy minimization, 50 ps of NVT molecular

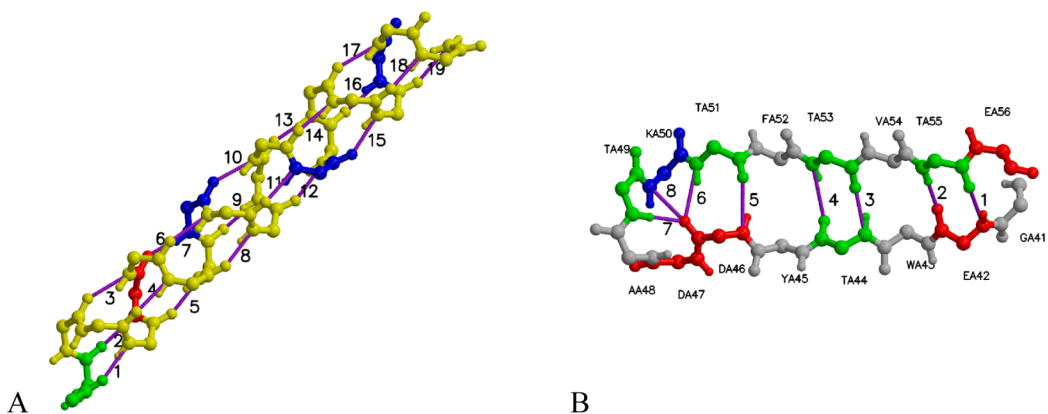


Figure 1. Folded structures of the two peptides, with backbone hydrogen bonds shown as purple lines. (A) Backbone atoms of WH21 peptide (Ala in yellow, Trp in green, His in red, Arg in blue). HB1 is formed by the carbonyl O of the acetyl blocking group with the peptide N–H of residue 4, and HB19, by the carbonyl O of residue 18 with the NH₂ of the blocking amide group. (B) Backbone atoms of GB1 peptide (nonpolar residues in gray, polar in green, acidic in red, basic in blue). Hydrogen bonds are numbered starting from the peptide termini and ending with HB7 and HB8 in the turn region.

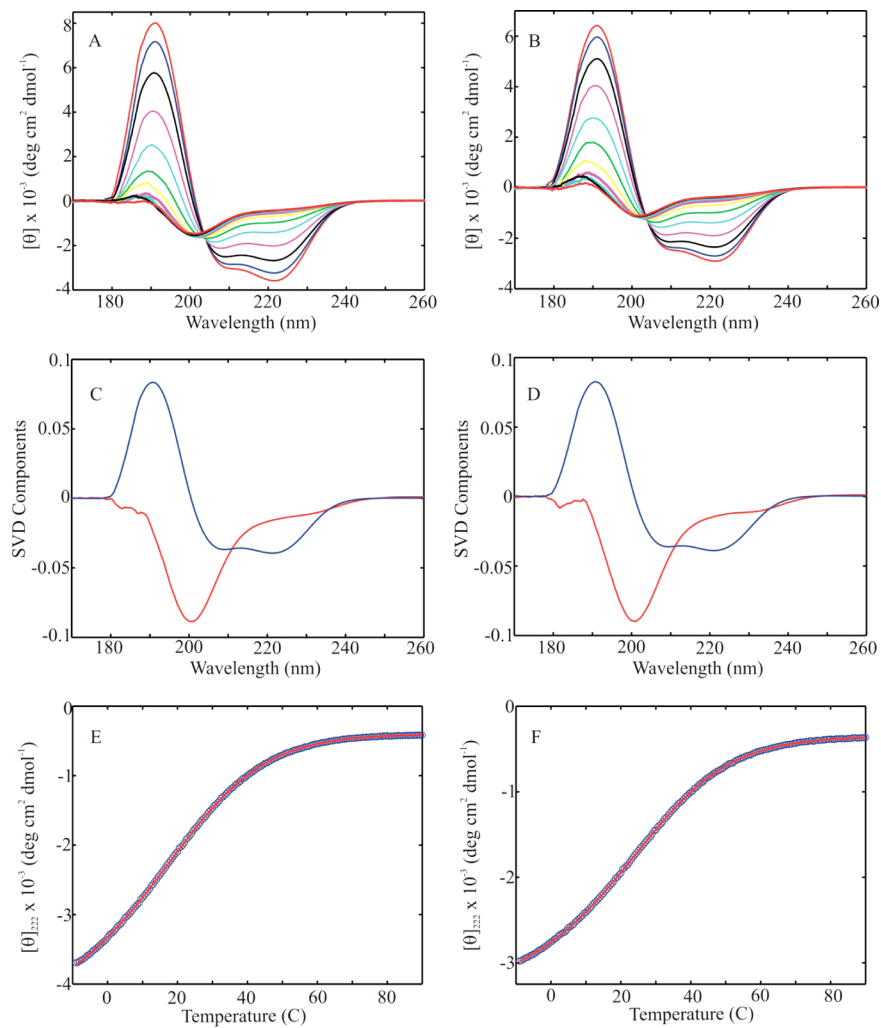


Figure 2. Far UV CD and SVD of dansylated and non-dansylated W₁-H₅-21. (A) Far UV CD of W₁-H₅-21 from 266 to 363 K. (B) Far UV CD of dan-W₁-H₅-21 from 266 to 363 K. (C) SVD analysis of W₁-H₅-21 indicates two main spectral components: (1) Blue - typical of an α -helix with a maximum around 190 nm and two minima around 208 and 222 nm. (2) Red - random coil-like structure with a minimum around 200 nm. (D) SVD analysis of dan-W₁-H₅-21 indicates two main spectral components identical to non-dansylated W₁-H₅-21. (E) Melting curve of W₁-H₅-21 from far UV CD with the EXAM fit shown in red. (F) Melting curve of dan-W₁-H₅-21 from far UV CD with the EXAM fit shown in red.

dynamics with positional restraints on the peptide at 300 K and 100 ps unrestrained NPT MD at 300 K and 1 bar, after which

the final size of the cubic solvent box was 45.0 Å. The final structure was used to start an 800 ns constant volume replica-

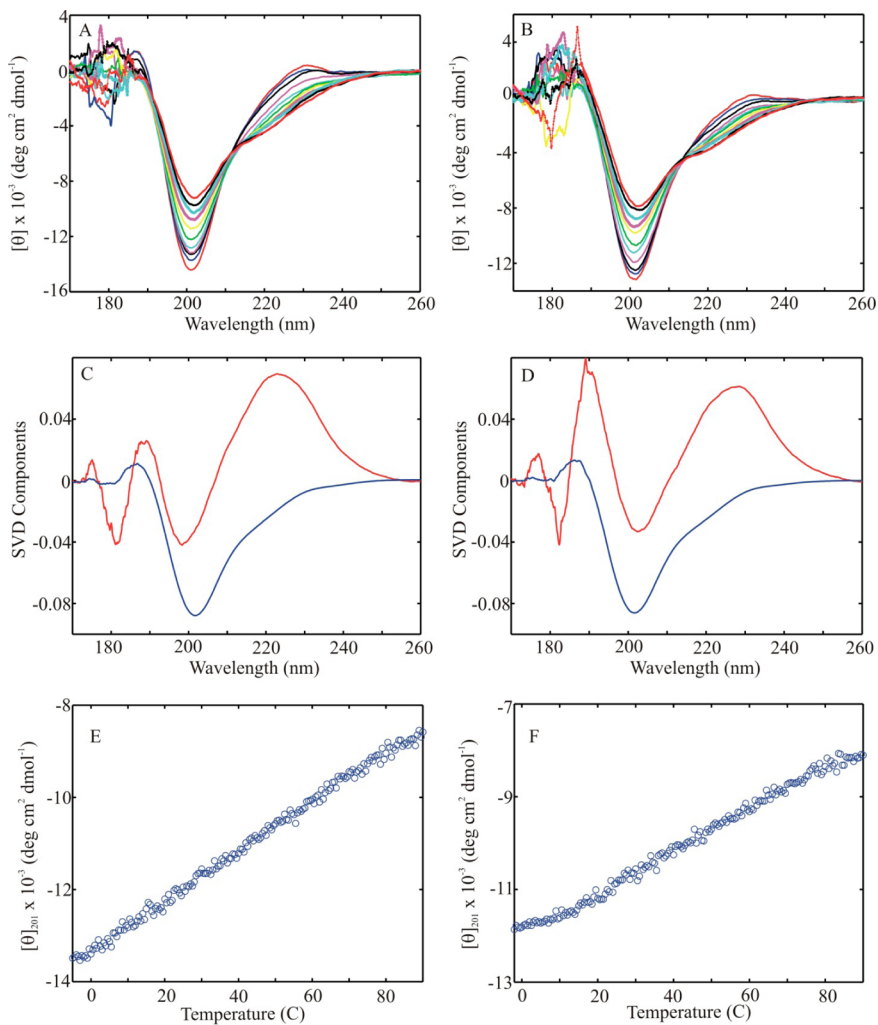


Figure 3. Far UV CD and SVD of dansylated and non-dansylated β -hairpin. (A) Far UV CD of β -hairpin from 266 to 363 K. (B) Far UV CD of dansylated β -hairpin from 266 to 363 K. (C) SVD analysis of β -hairpin indicates two main spectral components: (1) Typical of a β -turn conformation with a minimum around 200 nm. (2) Random coil-like structure with a minimum around 198 nm. (D) SVD analysis of dansylated β -hairpin also indicates two main spectral components: (1) Blue - Typical of a β -turn conformation with a minimum around 200 nm. (2) Red - random coil-like structure with a minimum around 198 nm. (E) Melting curve of β -hairpin from far UV CD. (F) Melting curve of dansylated β -hairpin from far UV CD.

exchange MD simulation. 40 replicas with temperatures in the 300–500 K range were employed, with exchange attempts every 1 ps and average acceptance ratios in the 0.17–0.32 range. The REMD simulations were carried out with constraints on all bonds, with an integration time step of 2 fs. The trajectory generation rate was about 30 ns/day running on 8 cores/replica on the Kodiak cluster at Baylor University.

Force Fields. We performed REMD simulations using AMBER03,⁴² CHARMM27,³⁹ and OPLS/AA⁴³ potentials for both WH21 and GB1 peptides. The general description of the WH21 results has been presented before.²⁶ As seen previously, the potentials differed significantly in their predictions.⁴⁴ AMBER03 tended to underestimate hairpin stability, while CHARMM27 tended to overestimate helix populations. In turn, OPLS/AA overestimated hairpin and underestimated helix stabilities. In the end, only the AMBER03 WH21 and CHARMM27 GB1 simulations generated significant changes in folded state populations in the simulated temperature range, and thus they were chosen to model the temperature changes of the FRET signal.

Simulation Analysis. Our primary focus is on analyzing hydrogen bonds, for which we present a novel pattern analysis. Due to the presence of the terminal blocking groups, W₁H₅–21 can form 19 α -helical hydrogen bonds. Counting from the N-terminus, HB1 is formed between the carbonyl oxygen of the N-terminal blocking group and the peptide NH of Ala 4, and HB19 is formed between the carbonyl oxygen of Ala 18 and the nitrogen atom of the C-terminal blocking group (Figure 1A). To generate WH21 melting curves, the helix content is evaluated as NHB/19, where NHB is the number of helical hydrogen bonds with O···C distances below 3.6 Å (HB method), or as NPP/21, where NPP is the number of residues with (φ , ψ) dihedrals within 20° of the ideal helix conformation (-62° , -41°) (PP method). For the initial structure of GB1–16, analysis with STRIDE⁴⁵ yields eight backbone hydrogen bonds, of which six (HB1–HB6) form the β -hairpin structure and two (HB7 and HB8) are part of the central turn (Figure 1B). Our GB41–56 hydrogen bond pattern thus differs slightly from previous studies. For the GB1 melting curve, hairpin content was measured as NHB/6, where NHB is the number of hairpin bonds with O···N distances below 3.6 Å. Additional

properties considered for both peptides include the root-mean-square deviation from the folded structure, radius of gyration, and end-to-end distance. For GB41–56, we also analyzed the trajectory populations of native residue contacts. For seven $\text{Ca}\cdots\text{Ca}$ pairs, we considered the contact formed when the corresponding interatomic distance is below 6 Å, and for six side chain–side chain contacts, we employed a cutoff of 8 Å for distances between side-chain centers (Figure S12, Supporting Information). Analyses of statistical uncertainty are primarily based on dividing the relevant data into 10 blocks and calculating the standard deviation of the mean, scaled by the appropriate *t*-coefficient.

RESULTS AND DISCUSSION

Circular Dichroism. The far UV CD spectra of the α -helix and β -hairpin were recorded as a function of temperature between 266 and 363 K (Figures 2 and 3). Analysis of the data provides information on the secondary structure of the peptides and confirms that the addition of the dansyl acceptor group does not markedly alter their overall structures.

Far UV CD spectra of both forms of W₁-H₅-21 are shown in Figure 2A and B. Singular value decomposition (SVD) was applied to the CD data to resolve the spectral components (Figure 2C and D), and two well-resolved components were identified for the W₁-H₅-21 peptides. The first component of both the dansylated and non-dansylated W₁-H₅-21 peptides shows two minima near 208 and 222 nm and a maximum at 190 nm, typical of helical secondary structure. The second components show a minimum near 200 nm, indicating the presence of random-coil-like structures. All other SVD components recovered noise and could not be resolved into additional structural elements. The melting curves of each helical system were found by scanning the temperature at a fixed wavelength of 222 nm. A two-state fit to the temperature unfolding curve of both dansylated and non-dansylated W₁-H₅-21 (Figure 2E and F) showed a melting temperature of 295 and 289 K with an enthalpy change of -17.7 and -16.5 kcal/mol, respectively. The thermodynamic parameters for the folding transition are presented in Table 1, demonstrating that dansylation slightly shifted the equilibrium toward the folded form at 298 K. This collection of data is important because it indicates that our systems were designed correctly to study the helical secondary structure and addition of the dansyl acceptor does not perturb this secondary structure

Table 1. Thermodynamic Parameters for the Folding Transition of Non-Dansylated and Dansylated W₁-H₅-21 Obtained from the Two-State Fit of the Circular Dichroism Data^a

	pH 4.8	
	W ₁ -H ₅ -21-nd	W ₁ -H ₅ -21-d
T _m (K)	288.8	295.3
ΔH° (kcal/mol)	-16.5	-17.7
ΔS° (cal/mol·K)	-57.2	-59.8
ΔG ₂₉₈ ° (kcal/mol·K)	0.52	0.16
K ₂₉₈	0.41	0.76
f ₂₉₈	0.29	0.43

^aΔH, enthalpy change; ΔS, entropy change; ΔG₂₉₈, K₂₉₈, and f₂₉₈, free energy change, equilibrium constant, and helix fraction at 298.15 K; T_m, midpoint transition. The errors are about 5% of the calculated thermodynamic quantities.

The temperature-dependent far UV CD spectra for the non-dansylated and dansylated β -hairpin are shown in Figure 3A and B. Singular value decomposition (SVD) was applied to the CD data to resolve the structural components present. Two well-resolved components were found and were similar for both forms of the peptide (Figure 3C and D). The first component indicates a β -turn-like structure with minima at about 200 nm. This is expected, since the hairpin is formed via a turn-like segment. The second component contains a minimum at about 198 nm, typical of a random-coil-like structure. Also, there is a maximum at about 230 nm which could be indicative of a PPII conformation. The melting curves were measured at 201 nm as a function of temperature. These curves could not be fit to a two-state model; therefore, the thermodynamic parameters for the β -hairpin peptides could not be deduced.

FTIR. A qualitative estimate of the secondary structural elements of the dansylated and non-dansylated peptides was obtained by decomposition of the FTIR amide I band into its constituent components. The secondary structural content of dansylated and non-dansylated W₁-H₅-21 and β -hairpin with a 5% error is shown in Figure 4. The non-dansylated W₁-H₅-21 (Figure 4C) contains a peak consisting of 41% α -helix (1654 cm⁻¹), a peak at 1626 cm⁻¹ indicating 15% β -sheet content, a peak at 1679 cm⁻¹ indicating a turn (19%), and a peak (1641 cm⁻¹) indicating 24% random coil. The dansylated W₁-H₅-21 (Figure 4D) contains a peak indicating 31% α -helix (1654 cm⁻¹), a peak at 1625 cm⁻¹ indicating 16% β -sheet content, a peak at 1677 cm⁻¹ indicating a turn (23%), and a peak (1640 cm⁻¹) suggesting 30% random coil. The non-dansylated β -hairpin (Figure 4A) contains peaks at 1621, 1636, and 1684 cm⁻¹ implying 49% β -sheet, at 1665 cm⁻¹ indicating 24% turns, and a peak at 1650 cm⁻¹ indicating 27% random coil. The dansylated β -hairpin (Figure 4B) consists of peaks at 1622, 1636, and 1681 cm⁻¹ suggesting 55% β -sheet, at 1666 cm⁻¹ indicating 16% turns, and a peak at 1650 cm⁻¹ showing 29% random coil. Therefore, structural analysis of the FTIR measurements is in agreement with the far UV CD results, further supporting the stability of these peptides upon the addition of the dansyl acceptor group.

FRET. Förster resonance energy transfer provided a means of estimating the distance between the Trp–dansyl donor–acceptor pair. These results provide insight into the formation of the two major secondary structure types (Figures 5 and 6). Due to the location of the donor and acceptor dyes, our measured donor–acceptor distances are representative of the end-to-end distances of the two peptides.

The UV fluorescence spectra of non-dansylated (Figure 5A) and dansylated (Figure 5B) W₁-H₅-21 are used to calculate the FRET efficiency over the temperature range 268–363 K. The results are converted to a plot of average donor–acceptor distance vs temperature (Figure 5C) using eq 1. Interestingly, the system exhibits an increase of FRET efficiency (*E*) between 268 and 298 K, followed by a decrease of *E* between 298 and 363 K. Thus, in the course of the thermal unfolding of W₁-H₅-21-dans, the donor–acceptor distance starts just above 22.0 Å at 268 K and exhibits a small but statistically significant decrease to 21.5 Å at 298 K, before expanding to about 24.5 Å at the highest temperature of 363 K. We emphasize that these distances are only estimates due to the assumption of $\kappa^2 = 2/3$, but most importantly here, the relative changes in distances remain significant.

The non-monotonic variation of peptide size with temperature provides interesting information about the helix unfolding

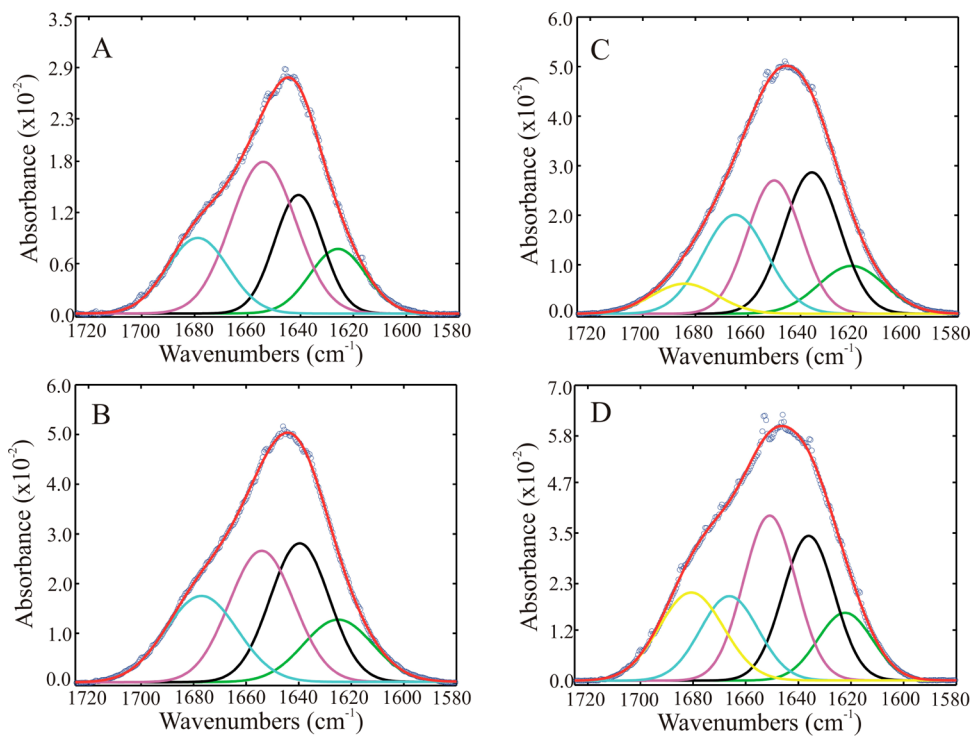


Figure 4. FTIR of dansylated and non-dansylated $W_1\text{-}H_5\text{-}21$ and β -hairpin: (A) non-dansylated β -hairpin; (B) dansylated β -hairpin; (C) non-dansylated $W_1\text{-}H_5\text{-}21$; (D) dansylated $W_1\text{-}H_5\text{-}21$.

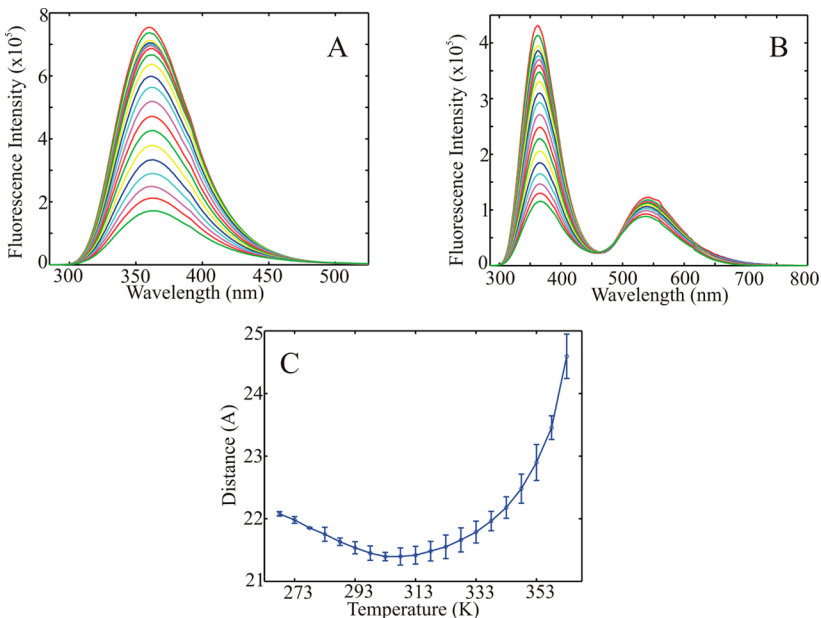


Figure 5. Fluorescence spectra of the dansylated and non-dansylated $W_1\text{-}H_5\text{-}21$ peptide measured from 268 to 363 K and the distance between the donor–acceptor pair calculated for each temperature: (A) fluorescence spectra of non-dansylated $W_1\text{-}H_5\text{-}21$; (B) fluorescence spectra of dansylated $W_1\text{-}H_5\text{-}21$; (C) distance between donor–acceptor pair as a function of temperature.

pathway. This picture is inconsistent with a simple model of shifting equilibrium between the two fixed families of conformations, folded and unfolded. Rather, our FRET results suggest that in the early stages of unfolding the peptide populates structures that are shorter than the helical form, while in the later stages it takes on conformations of larger size. The initial decrease of peptide size with increasing temperature is consistent with previous SAXS studies.⁷ That work showed that, at low temperature, helix-forming peptides tend to have a

radius of gyration that is shorter than an ideal α -helix. This was explained by suggesting that the peptides form broken helix type conformations, even though CD or NMR measurements indicated the presence of fully helical structures.⁷

The UV fluorescence spectra of non-dansylated (Figure 6A) and dansylated GB41–56 (Figure 6B) were used to calculate the FRET efficiency and average donor–acceptor distance (Figure 6C) in the temperature range 268–363 K. The GB1–16 donor–acceptor distance exhibits a linear increase from just

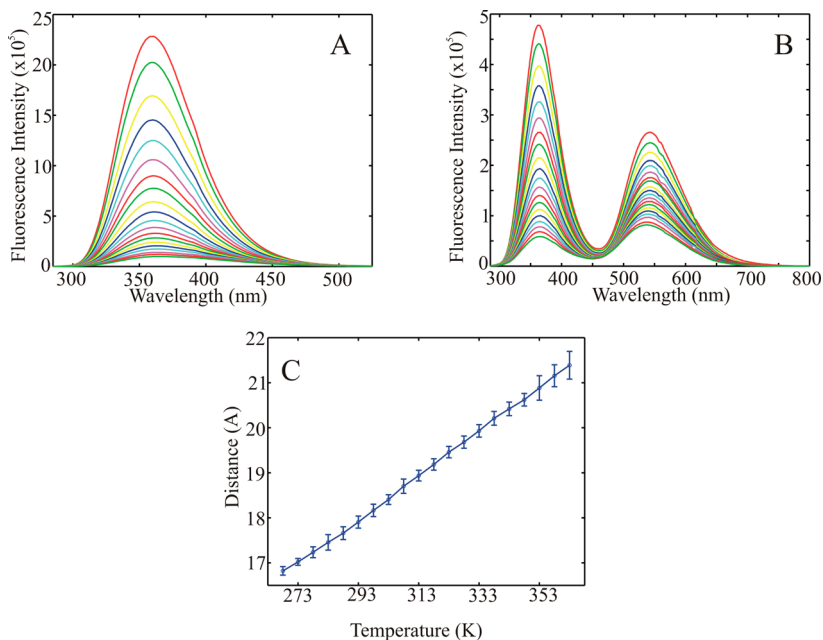


Figure 6. Fluorescence spectra of the dansylated and non-dansylated β -hairpin peptide measured from 268 to 363 K and the distance between the donor–acceptor pair calculated for each temperature: (A) fluorescence spectra of non-dansylated β -hairpin; (B) fluorescence spectra of dansylated β -hairpin; (C) distance between donor–acceptor pair as a function of temperature.

below 17 Å at 268 K to about 21.5 Å at 363 K. The FRET measurements thus indicate that the β -hairpin end-to-end distance increases monotonically with increasing temperature as the peptide unfolds. Thus, our measurements show that the unfolded state is characterized by a larger size (end-to-end distance) than the folded β -hairpin. This new experimental information confirms intuitive expectations, and is in accord with the proposed models of β -hairpin unfolding, including the zipper-like models.

Overall, our FRET experiments have provided interesting new information about the pathways of α -helix and β -hairpin folding. The two secondary structures exhibited markedly different changes in end-to-end distance with temperature. For the α -helix, the results suggest an initial decrease and then an increase of size, while for the β -hairpin we detected a monotonic increase in size as the temperature was raised. In the following sections, we provide explanations of this behavior in terms of the structures sampled in REMD simulations of the two peptides.

Simulations of W₁H₅-21 Helix. The results of our 1 μ s AMBER03 REMD simulation of the W₁H₅-21 peptide are described below. The basic description of this simulation has been presented previously, with a focus on comparing helix folding predictions of different force fields.²⁶ Here we present a brief summary of the main results, concentrating on analyzing aspects that were not previously discussed and those related to the new experimental data presented in this work. The simulation appears to have converged within the first 100 ns (Figure S1, Supporting Information), so we present results from the complete trajectory.

Melting Curves. Melting curves have been generated on the basis of distributions of populations of α -helical hydrogen bonds and backbone (φ , ψ) dihedrals, as described in the Methods section (Figure 7A). These curves show an α -helix population of 61–63% at 300 K.²⁶ Fitting to a two-state model gives thermodynamic parameters for helix folding: $T_m = 345$ K, $\Delta H = -4.3$ kcal/mol, and $\Delta S = -13.0$ cal/(mol K) from the dihedrals.

The simulations yield qualitatively correct results for melting, with signs for enthalpy and entropy changes in accord with observations. Quantitatively, the calculated ΔH , ΔS , and T_m values are significantly different from experimental data.

Hydrogen Bond Distributions. Figure 7B shows the distribution of the overall number of hydrogen bonds (NHB) in sampled structures. Except for the highest temperatures, the majority of the structures correspond to intermediate stages of folding, with NHB in the 7–12 range. Figure 7C shows the populations of the individual hydrogen bonds as a function of temperature. Generally, the lowest populations are at the termini and in the central part of the helix, with peaks for HB1, HB6, and HB11–HB16.²⁶ Statistically, the unfolding process starts at the termini, proceeds through the intermediate “island of stability” involving HB11–HB16, and exhibits a pattern of enhanced stability of several individual hydrogen bonds that are structurally close to the nonalanine residues (Figures 7C and S3, Supporting Information). The HB11–HB16 intermediate is in the central region of the peptide but is markedly shifted toward the C-terminus.

Measures of Size and Shape. Simple measures of global size and shape of the peptide are provided by the end-to-end distance (Figure 7D) and radius of gyration (Figure S4A, Supporting Information). With increasing temperature, the average end-to-end distance exhibits a definite “U”-shaped response, decreasing in the 290–380 K range and increasing at higher temperatures. The radius of gyration exhibits a slight decline in average value as the temperature rises from 290 to 370 K, followed by an increase at higher temperatures (Figure S4A, Supporting Information). In contrast, both the global measure of the average RMSD from helix and the local measure of the distance between the side chains of Trp1 and His5 exhibit a systematic increase with temperature (Figures S4B and C, Supporting Information).

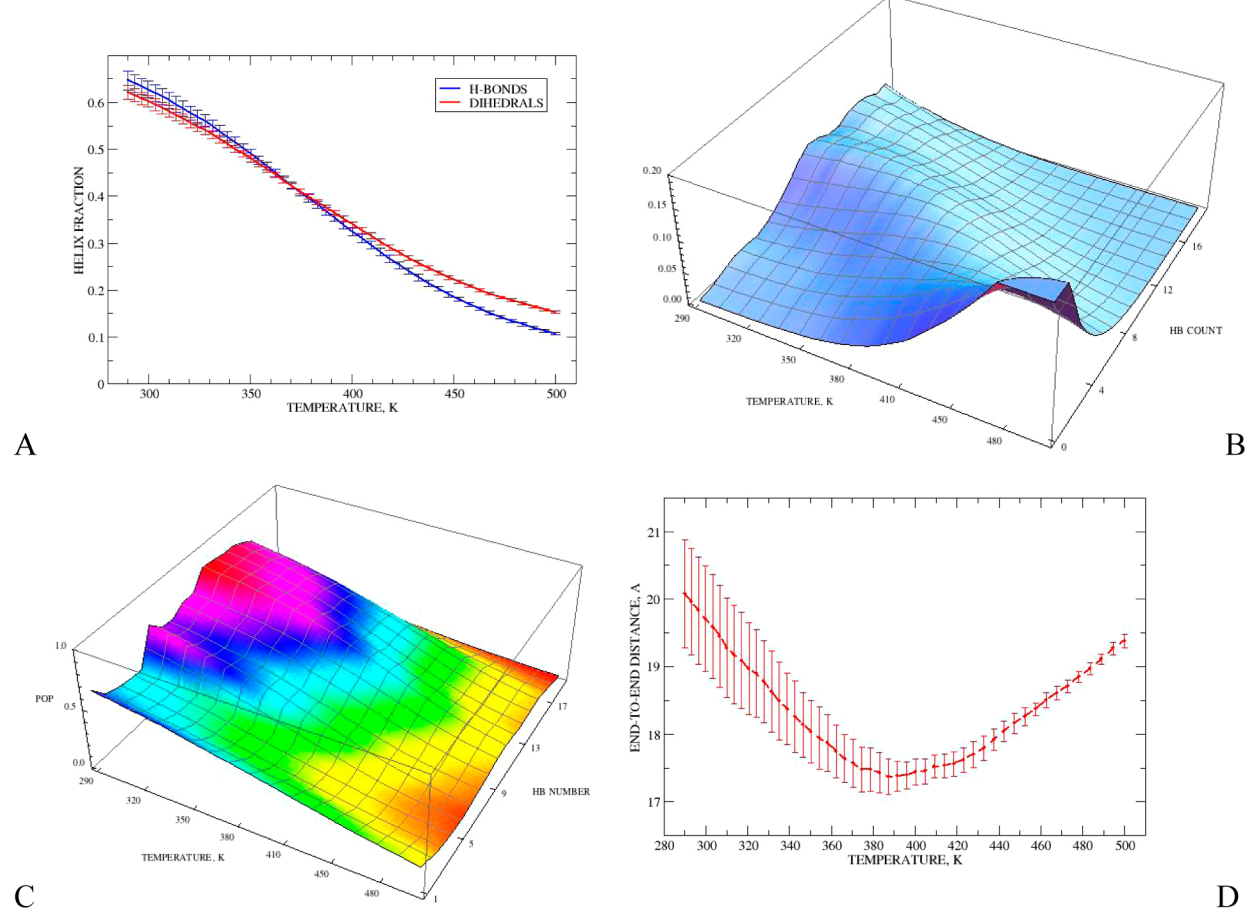


Figure 7. (A) Melting curves calculated from 1 μ s WH21 peptide REMD simulation with AMBER03. H-bonds - based on the fraction of formed α -helical bonds (HB method), dihedrals - based on the fraction of residues in the α -helical region of the Ramachandran map (PP method). (B) Distribution of the total number of formed α -helical hydrogen bonds as a function of temperature. (C) Populations of the 19 individual α -helical hydrogen bonds as a function of temperature. Numbering as in Figure 1A. (D) Average end-to-end distance as a function of temperature. A, D - The error bars indicate 95% confidence interval of the mean.

Cluster Analysis. Clustering of the structures was performed for the 300, 340, and 500 K replicas, yielding 514, 1659, and 17 126 clusters, respectively. The major sampled structures correspond to helices with minor fraying at the termini and compact structures with either helix-turn-helix motifs or to a state with unfolded N-terminal interacting with a C-terminal helix (Figure S5, Supporting Information).

Helix Fragments. Statistics of helix fragments, defined as segments with at least three consecutive helical hydrogen bonds, are shown in Figure 8A and Table S1 (Supporting Information). At the lowest temperatures, the majority of structures sampled (ca. 80%) represent single helices, with a minor population of two-helix (ca. 15%) and coil (5%). At T_m , the population of single helices falls to ca. 70%, while those of two-helix structures and coils increase to 18 and 12%, respectively. At the highest temperatures, coil forms dominate. There is also a low (below 0.6%) population of three-helix structures and a tiny presence of four-helical forms (below 5×10^{-5}).

Helix Folding Pathway. Our analysis yields a microscopic picture of the statistical WH21 helix folding pathway. The helix is initiated independently at several locations: HB1, HB6, HB11, and HB16. The next stage is formation of the “island of stability”, involving HB11–16, followed by extension of the helix population in the central region of the peptide, in which

both single-helix and two-helix structures appear. The final stage involves forming hydrogen bonds at the termini of a single central helix. The dominant feature is sampling a large range of intermediate conformations. The free energy landscape of WH21 at 300 K is shown in Figures 8B and S6 (Supporting Information). As discussed previously,²⁶ the AMBER03 landscape corresponds to a two-state system, with a barrier of less than 1 kcal/mol separating the folded and unfolded basins.

Insight into the “U” shape of the size vs temperature plots is presented in Figure 8C, in which the sizes of coil, single-helix, and helix-turn-helix states are analyzed. This data shows that the shape is primarily due to the behavior of the single-helical structures. Evidently, as the ends of the helix become progressively frayed with increasing temperature, the initial result is a decrease in size, followed by an increase. This determines the shape of the size vs T plots below T_m , where the single-helical motifs dominate. The coil states show a strong systematic increase of size with temperature, starting markedly below the helices and reaching similar (in end-to-end distances) or higher (radius of gyration) values at 500 K. This property determines the shape of the distance vs T plots above T_m , where the coils are the dominant species.

Comparison with Previous Simulations. Our results are in good qualitative agreement with previous explicit solvent simulations for A21 and F₈ peptides from the Garcia²² and

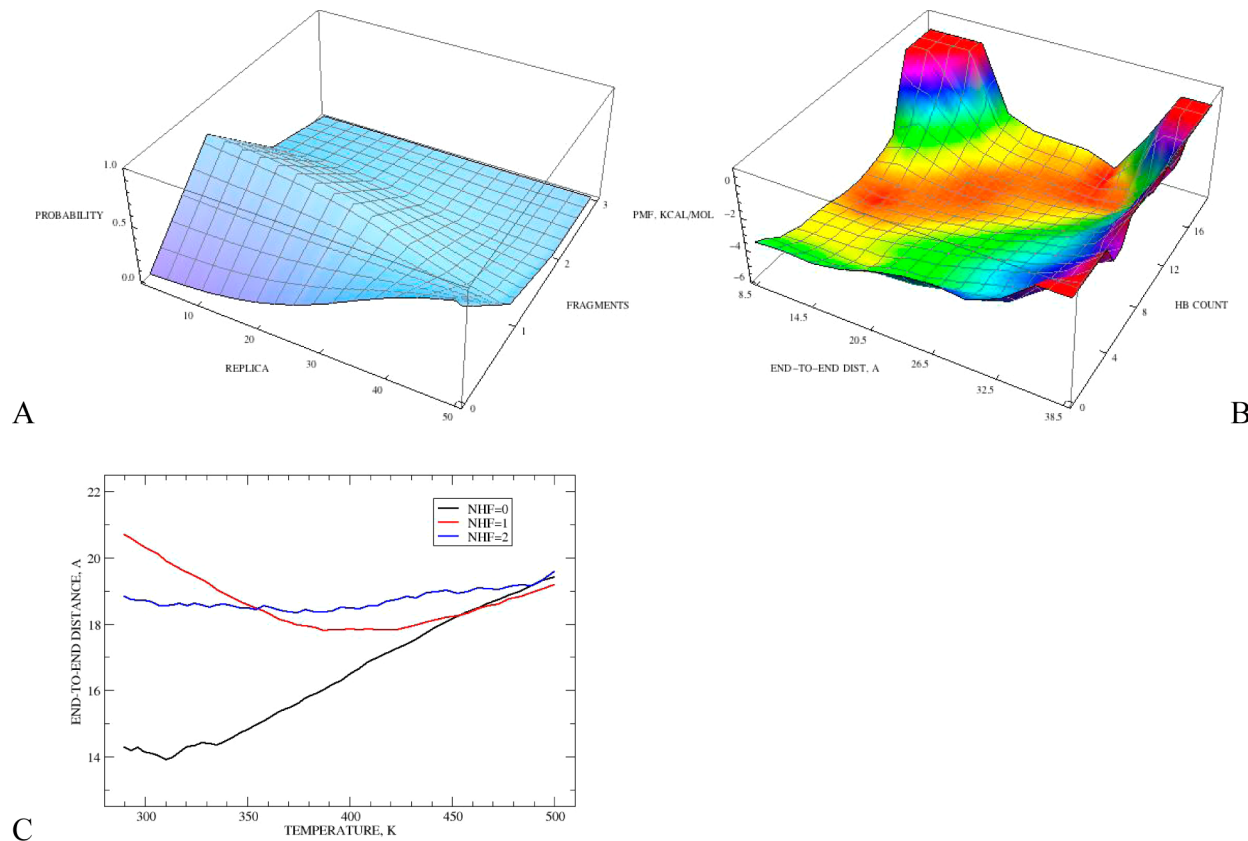


Figure 8. $1\ \mu\text{s}$ WH21 peptide REMD simulation with AMBER03: (A) Distribution of the number of helix fragments vs temperature. The temperature ranges from 290 K for replica 1 to 500 K for replica 50. A helix fragment is defined as a segment of at least three consecutive α -helical $i \cdots i + 4$ hydrogen bonds. (B) Free energy landscape in coordinates of end-to-end distance vs NHB (number of formed α -helical hydrogen bonds). (C) Average end-to-end distance as a function of temperature separated into subclasses of structures with 0, 1, and 2 helix fragments.

Pande²³ groups. The melting curve calculated in this work (Figure 7A) is comparable to the “modified” curve for the Fs peptide.²⁵ Both overall helix fraction and individual hydrogen bond populations are lower in our study than Garcia’s results. Our individual hydrogen bond populations (Figure 7C) are roughly comparable to results of Garcia and Pande.²³ The number of helical fragments found in our work is lower than seen previously.^{22,23} Our pathway for helix folding is partly consistent with the network model derived by Pande.²³ We also find two conformational basins (folded and unfolded), multiple nucleation sites, and intermediate structures with one and two helical fragments. The main difference is that in our work structures with three helical fragments are a very small fraction of observed forms at 300 K (ca. 0.4%), while they appear to be much more highly populated and play important roles in the folding kinetics elsewhere.²³

Comparison with Experimental Data. Our simulations generally tend to overestimate helix stability. The calculated helix content at 300 K is 63%, about 2 times higher than the 29% from CD measurements at 298 K (on the basis of the equilibrium constant of 0.41 in Table 1). The calculated melting temperature is overestimated by about 50 K, while ΔH and ΔS are underestimated by a factor of 5–6 compared to Table 1. The observed non-monotonic variation of peptide size with temperature is correctly reproduced by simulations, which suggest that the effect may be explained primarily by helix fraying at the ends. The low calculated free energy barrier between the folded and unfolded basins is also in accord with experimental data.⁴⁶

GB41–56 Hairpin Simulations. The results of our REMD simulations of the GB41–56 peptide using the CHARMM force field are described below. We present the results from the last 400 ns of the 800 ns trajectory, over which the simulation has converged (Figure S7, Supporting Information).

Melting Curve. The melting curve has been generated on the basis of distributions of populations of the six β -hairpin hydrogen bonds HB1–HB6 (Figure 9A). The curves show a β -hairpin population of about 70% at 300 K. Fitting to a two-state model gives thermodynamic parameters: $T_m = 354$ K, $\Delta H = -8.3$ kcal/mol, and $\Delta S = -23$ cal/(mol K). Our calculated hairpin population falls above experimental estimates of 30–50%.¹⁶ Below, we analyze the microscopic details of the unfolding pathway extracted from the REMD data.

Hydrogen Bond Distributions. The trajectory populations of the six β -hairpin hydrogen bonds (HB1–HB6 in Figure 1B) are shown in Figures S8 and S15 (Supporting Information). At the lower temperatures, the most populated structures have six (35% population) and five (30%) hairpin hydrogen bonds. With increasing temperature, these populations decrease, while the population of the state with zero hairpin hydrogen bonds systematically increases from 20% at 300 K to 96% at 500 K. The population of intermediates generally remains low: at 300 K, structures with NHB = 4, 3, 2, and 1 have populations of only 10, 2, 0.04, and 0.03%, respectively.

Figure 9B shows populations of the six individual hairpin hydrogen bonds HB1–HB6 within subsets of structures with a given total number of hydrogen bonds, NHB = 0–6. The

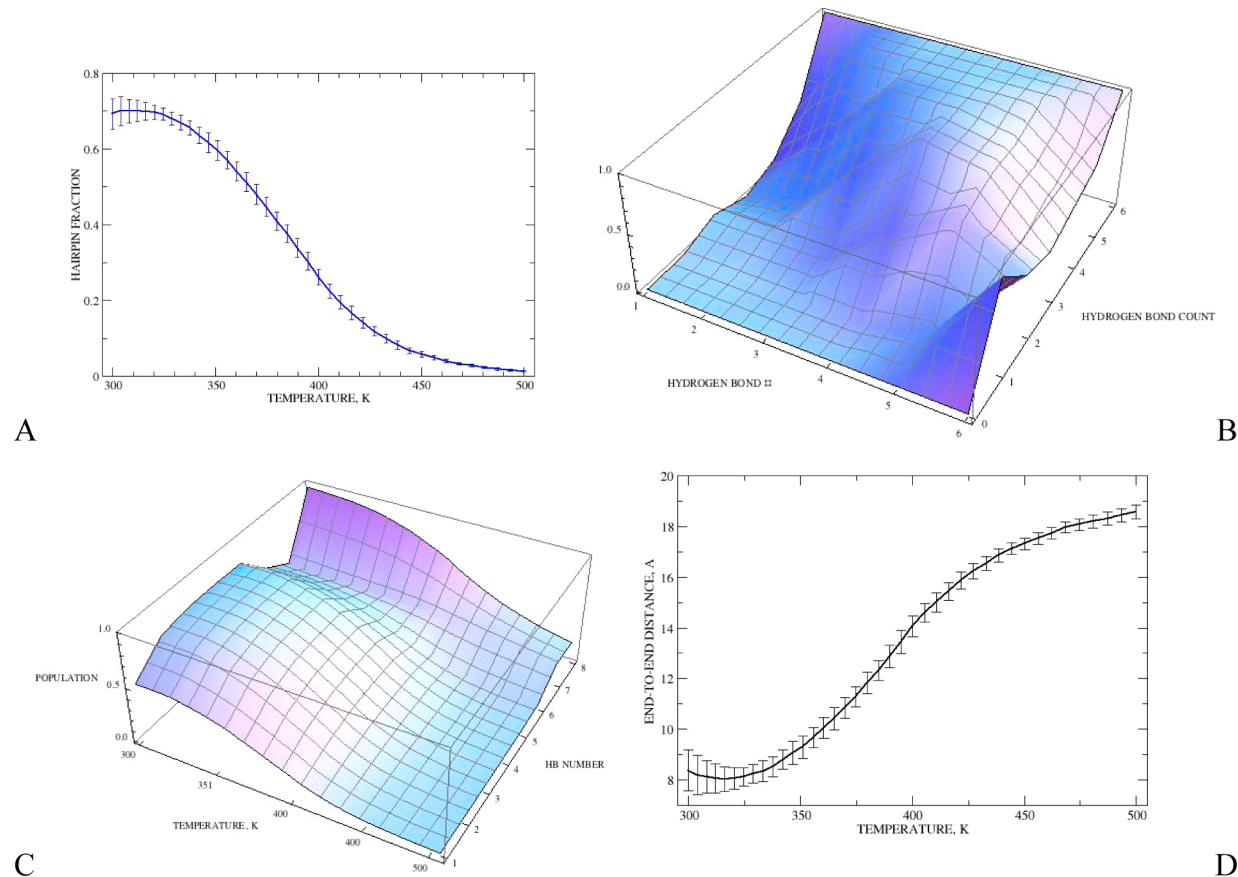


Figure 9. 800 ns GB1–16 β -hairpin REMD simulation with CHARMM27. (A) Melting curve based on the fraction of formed β -hairpin hydrogen bonds. (B) Populations of the six individual β -hairpin hydrogen bonds HB1–HB6, averaged over structures with different total numbers of formed hydrogen bonds (Figure 1B). (C) Populations of all eight individual GB1 hydrogen bonds as a function of temperature, including HB7 and HB8 in the turn region (numbering as in Figure 1B). (D) Average end-to-end distance as a function of temperature. Error bars indicate a 95% confidence interval of the mean.

progress from folded to unfolded form starts by loss of the hydrogen bond HB1 at the end of the hairpin and partial loss of HB6 at the turn. This is followed by a systematic loss of further hydrogen bonds from the end of the hairpin (HB2–HB5) and finally HB6. The populations of the intermediates with NHB = 1 and 2 are very low, in accord with the high entropic cost of hairpin initiation. Figure 9C shows the populations of all eight GB1 hydrogen bonds HB1–HB8 as a function of temperature. The central hydrogen bonds, HB2–HB5, exhibit systematically the highest populations, while HB1 and HB6, at the ends of the hairpin, have the lowest. As the temperature increases, the hydrogen bond populations decrease uniformly. Additional data are shown in the Supporting Information.

Turn Population. The populations of the two hydrogen bonds in the turn are 40% (HB7) and 97% (HB8) at 300 K, falling to about 18% for both bonds at 500 K (Figure 9C). Thus, HB8 is the most stable of all the backbone hydrogen bonds, and the turn is the most stable element of the hairpin. Pattern analysis for all eight backbone hydrogen bonds (Figures S8 and S9, Supporting Information) shows that the nucleation of the β -hairpin occurs by HB6 formation in a state with an already formed turn.

Residue Contacts. Figures showing patterns of backbone and side-chain atom contacts are given in Figure S11 (Supporting Information). The backbone $C\alpha$ – $C\alpha$ contacts parallel the formation of hydrogen bonds described above. Thus, the turn contact (ASP47–LYS50) has the highest

population, and is the one formed before any others, in parallel with the turn hydrogen bond HB8. On average, further contacts are added in a zipper-like model, propagating from the turn to the termini. In structures with intermediate numbers of contacts, the highest populations (besides ASP47–LYS50) are for the central residues TRP43–VAL54, THR44–THR53, and TYR45–PHE52. The side-chain contacts are initiated by the two hydrophobic pairs, TRP43–VAL54 and TYR45–PHE52. A low population of the TRP–PHE and ASP–LYS side-chain contacts is present before any hydrogen bonds (hairpin or turn) are formed. However, significant populations of native side chain contacts appear when at least three to four native hydrogen bonds are present.

Measures of Size and Shape. Simple measures of global size and shape of the GB1 peptide are provided by the end-to-end distance (Figure 9D) and radius of gyration (Figure S12, Supporting Information). Both plots show a similar trend, with the average peptide size remaining approximately constant in the 300–350 K range and a systematic increase at higher temperatures.

Cluster Analysis. Clustering of the structures was performed for the 300, 365, and 500 K replicas, yielding 84, 402, and 817 clusters, respectively (Figure S16, Supporting Information). At 300 K, the major sampled form corresponds to the folded hairpin. The major “unfolded” conformations are predicted to be coil-helix-coil motifs, with α -helices of various lengths and starting locations, mainly in the central turn region

of GB1. Populations of the partially formed hairpins, with NHB = 3 and below, are quite low. At 500 K, the dominant motifs are coil-helix-coil and coil. The most highly populated hairpin-like intermediates are shown in cluster 2 (NHB = 5, 2% population) and cluster 185 (NHB = 3, 0.2% population).

Secondary Structure. Analysis of the secondary structures performed using DSSP⁴⁷ shows that at 300 K the main elements are β -sheet (6.0 residues on average), turn (3.3 residues), and α -helix (1.9 residues). The β -sheet and turn content exhibit a systematic decrease with temperature, falling to 0.13 and 1.9 residues at 500 K, respectively, while the α -helix content varies in the 1.2–2.2 residue range (Figure S13, Supporting Information).

Hairpin Folding Pathway. Our data are consistent with the recently proposed broken zipper mechanism.¹⁶ The initial step is formation of the turn, involving first the ASP47…LYS50 side-chain contact and then the backbone contact and the turn hydrogen bond HB8. The next step involves propagation of hydrophobic contacts from the turn to the termini, with the hairpin hydrogen bonds being formed in parallel with contacts. The native-like packing of hydrophobic side chains TRP43…VAL54 and TYR45…PHE52 develops only after several hairpin hydrogen bonds have appeared. In terms of the β -hairpin hydrogen bonds, HB6 is formed first, followed by elongation to HB5, HB4, HB3, HB2, and HB1. Structures close to the hairpin, with 4–6 β -hairpin H-bonds, dominate at low temperatures and coils and coil-helix-coil motifs dominate at higher temperatures. Except for the turn, which is very stable, intermediates at the beginning of the folding path never reach high populations. The free energy landscape of GB1 is displayed in Figure S15 (Supporting Information), showing essentially two-state folding. Basins of folded and unfolded states are separated by a barrier of 3.4 kcal/mol, with the transition state corresponding to a folded-like structure (backbone RMSD 2–3 Å from hairpin), with three formed hydrogen bonds. Increased sampling of elongated unfolded states at higher temperatures leads to the increase of peptide length with increasing temperature (Figures 9D and S12, Supporting Information).

Comparison with Previous Simulations. Our CHARMM GB41–56 peptide simulations are in good agreement with previous computational studies. Our average hairpin hydrogen bond population of 70% at room temperature is within less than a factor of 2 from the 40–54% range found previously.^{27–30} Our hydrogen bond distribution (Figure S15, Supporting Information) is similar to the CHARMM simulations of Karplus.²⁷ Our distribution of populations of the individual β -hairpin hydrogen bonds is similar to that of Berne, obtained with OPLS/AA,^{28b} but differs in details from the results of Karplus (HB6 weakest, HB1–5 comparable²⁷) and Garcia (HB1 weakest, HB4–5 strongest^{28a}). While we find two minima on our various low-temperature 2D free-energy surfaces, Garcia^{28a} and Pande⁴⁸ found three, including a compact unfolded state, while Karplus²⁷ and Berne^{28b} obtained rougher landscapes. The presence of α -helical segments was also found by Berne,^{28b} Garcia,^{28a} and Best,⁴⁹ with the latter work also finding a zipper folding mechanism.

Comparison of Simulation Results with Experimental Data. The β -hairpin population estimated from REMD is 70% at 300 K, higher than the measured 30–50%.^{16,30} The melting temperature of GB1 has been estimated experimentally at 284–320 K.¹⁶ $T_m = 320$ K and $\Delta H = -48$ kcal/mol were determined for folding of a GB1 variant.⁵⁰ Thus, the REMD transition

temperature is overestimated by at least 30 K, while the transition enthalpy is underestimated by a factor of 6. The small partial α -helix content in the unfolded states is in qualitative agreement with NMR studies of a truncated eight-residue peptide derived from GB1.¹⁶ The changes of peptide end-to-end distance with temperature found in our simulations follow an S-shaped curve, which is somewhat different than the monotonic increase observed by FRET. Qualitatively, the hairpin behavior is different from that of the helical peptide, where both simulations and FRET found a U-shaped curve. The statistical picture of GB1 folding emerging from our REMD simulations is consistent with the broken zipper mechanism, which is supported by multiple lines of experimental evidence.¹⁶

CONCLUSIONS

We present here the results from a combined experimental and computational study of the microscopic unfolding pathways of α -helical and β -hairpin forming peptides. Our FRET measurements provide new data on variation of α -helix and β -hairpin size along the folding pathways, showing that the two secondary structures follow markedly different paths. The W₁H₅-21 helical peptide exhibits an initial decrease in length followed by an increase, while the GB41–56 hairpin shows a systematic increase in length as a function of increasing temperature. We also provide an analysis of the secondary structure of the peptides using CD and FTIR spectroscopy, yielding a new determination of the melting curve for W₁H₅-21 unfolding.

In the computational part of the project, we performed microsecond-length REMD simulations of the W₁H₅-21 and GB41–56 peptides, obtaining qualitative agreement between calculated and observed melting curves and yielding microscopic details of unfolding pathways. For the W₁H₅-21 helix, unfolding starts at the termini and proceeds through an off-center frayed helix. The unfolding intermediates, which dominate the conformational distribution, are primarily single helices with unwound termini and helix-coil-helix motifs. The simulations provided a qualitative reproduction of the experimentally observed variation of W₁H₅-21 length with temperature, explaining it as primarily due to the presence of frayed single-helix structures in equilibrium with coil conformers.

For the GB41–56 hairpin, our simulation results indicate that folding is initiated at the turn, with the population of the ASP47…LYS50 side-chain contact preceding formation of the turn hydrogen bond HB8. Next, the hairpin forms in a zipper-like fashion, with C α …C α contacts propagating from the turn to termini, and hairpin hydrogen bonds forming in parallel with these contacts. Native-like packing of the TRP43…VAL54 and TYR45…PHE52 side chains develops after several hairpin hydrogen bonds already appear. Intermediate structures have very low populations due to the entropic cost. Overall, the REMD results are in accord with the “broken zipper” model of Scheraga.¹⁶ Our simulation results qualitatively reproduce the monotonic increase of GB41–56 peptide size with increasing temperature determined from the FRET results in the experimental part of this work. The shape of the curve may be explained primarily by the zipper-like breaking of the hairpin hydrogen bonds and C α …C α contacts.

The FRET data give a projection of folding along a single coordinate from the multidimensional conformation space. The results of simulations are approximate, due to the simplified

nature of the potential energy functions used. Several studies have found that details of folding mechanisms exhibit a dependence on the employed force field.^{10,30,51} Additionally, our REMD results only provide statistics of conformer populations and not paths of actual conformational transitions. Thus, while our joint study has presented several novel features of folding for helices and hairpins, more experimental and computational investigations are needed to uncover the full picture of these complex and fascinating processes.

■ ASSOCIATED CONTENT

Supporting Information

Additional figures and tables describing details of the simulation data. This material is available free of charge via the Internet at <http://pubs.acs.org>.

■ AUTHOR INFORMATION

Corresponding Authors

*E-mail: 112gjas@uccaribe.edu.

*E-mail: kkuczera@ku.edu.

Notes

The authors declare no competing financial interest.

■ ACKNOWLEDGMENTS

G.S.J. would like to thank W. A. Eaton for helpful discussions. We acknowledge Baylor University Research Computer Services for computer time. G.S.J. also thanks Hector Maldonado for useful conversations. This project was supported in part by a subaward to DOE grant DOE DE-FG02-08ER46528 to K.K.

■ REFERENCES

- (1) Howlett, D. R. Misfolding in Disease: Cause or Response? *Curr. Med. Chem.: Immunol., Endocr. Metab. Agents* **2003**, *3*, 371–383.
- (2) (a) Schuler, B.; Eaton, W. A. Protein Folding Studied by Single-Molecule FRET. *Curr. Opin. Struct. Biol.* **2008**, *18* (1), 16–26. (b) Gopich, I. V.; Szabo, A. Theory of the Energy Transfer Efficiency and Fluorescence Lifetime Distribution in Single-Molecule FRET. *Proc. Natl. Acad. Sci. U.S.A.* **2012**, *109* (20), 7747–7752.
- (3) Thompson, P. A.; Munoz, V.; Jas, G. S.; Henry, E. R.; Eaton, W. A.; Hofrichter, J. The Helix-Coil Kinetics of a Heteropeptide. *J. Phys. Chem. B* **2000**, *104* (2), 378–389.
- (4) Jas, G. S.; Eaton, W. A.; Hofrichter, J. Effect of Viscosity on the Kinetics of Alpha-Helix and Beta-Hairpin Formation. *J. Phys. Chem. B* **2001**, *105* (1), 261–272.
- (5) Jas, G. S.; Kuczera, K. Equilibrium Structure and Folding of a Helix-Forming Peptide: Circular Dichroism Measurements and Replica-Exchange Molecular Dynamics Simulations. *Biophys. J.* **2004**, *87* (6), 3786–3798.
- (6) Ianoul, A.; Mikhonin, A.; Lednev, I. K.; Asher, S. A. UV Resonance Raman Study of the Spatial Dependence of Alpha-Helix Unfolding. *J. Phys. Chem. A* **2002**, *106* (14), 3621–3624.
- (7) Zagrovic, B.; Jayachandran, G.; Millett, I. S.; Doniach, S.; Pande, V. S. How Large Is an Alpha-Helix? Studies of the Radii of Gyration of Helical Peptides by Small-Angle X-Ray Scattering and Molecular Dynamics. *J. Mol. Biol.* **2005**, *353* (2), 232–241.
- (8) Lin, M. M.; Mohammed, O. F.; Jas, G. S.; Zewail, A. H. Speed Limit of Protein Folding Evidenced in Secondary Structure Dynamics. *Proc. Natl. Acad. Sci. U.S.A.* **2011**, *108* (40), 16622–16627.
- (9) Jas, G. S.; Hegefled, W. A.; Majek, P.; Kuczera, K.; Elber, R. Experiments and Comprehensive Simulations of the Formation of a Helical Turn. *J. Phys. Chem. B* **2012**, *116* (23), 6598–6610.
- (10) Hegefled, W. A.; Chen, S. E.; DeLeon, K. Y.; Kuczera, K.; Jas, G. S. Helix Formation in a Pentapeptide Experiment and Force-Field Dependent Dynamics. *J. Phys. Chem. A* **2010**, *114* (47), 12391–12402.
- (11) Huang, C. Y.; Getahun, Z.; Zhu, Y. J.; Klemke, J. W.; DeGrado, W. F.; Gai, F. Helix Formation Via Conformation Diffusion Search. *Proc. Natl. Acad. Sci. U.S.A.* **2002**, *99* (5), 2788–2793.
- (12) Ihlainen, J. A.; Paoli, B.; Muff, S.; Backus, E. H. G.; Bredenbeck, J.; Woolley, G. A.; Caflisch, A.; Hamm, P. Alpha-Helix Folding in the Presence of Structural Constraints. *Proc. Natl. Acad. Sci. U.S.A.* **2008**, *105* (28), 9588–9593.
- (13) Blanco, F. J.; Jimenez, M. A.; Pineda, A.; Rico, M.; Santoro, J.; Nieto, J. L. NMR Solution Structure of the Isolated N-Terminal Fragment of Protein-G B1 Domain. Evidence of Trifluoroethanol Induced Native-Like Beta-Hairpin Formation. *Biochemistry* **1994**, *33* (19), 6004–6014.
- (14) Munoz, V.; Thompson, P. A.; Hofrichter, J.; Eaton, W. A. Folding Dynamics and Mechanism of Beta-Hairpin Formation. *Nature* **1997**, *390* (6656), 196–199.
- (15) (a) DeAlba, E.; Rico, M.; Jimenez, M. A. Cross-Strand Side-Chain Interactions Versus Turn Conformation in Beta-Hairpins. *Protein Sci.* **1997**, *6* (12), 2548–2560. (b) Ramirez-Alvarado, M.; Kortemme, T.; Blanco, F. J.; Serrano, L. Beta-Hairpin and Beta-Sheet Formation in Designed Linear Peptides. *Bioorg. Med. Chem.* **1999**, *7* (1), 93–103. (c) Espinosa, J. F.; Syud, F. A.; Gellman, S. H. Analysis of the Factors That Stabilize a Designed Two-Stranded Antiparallel Beta-Sheet. *Protein Sci.* **2002**, *11* (6), 1492–1505. (d) Fesinmeyer, R. M.; Hudson, F. M.; Andersen, N. H. Enhanced Hairpin Stability through Loop Design: The Case of the Protein G B1 Domain Hairpin. *J. Am. Chem. Soc.* **2004**, *126* (23), 7238–7243. (e) Haque, T. S.; Gellman, S. H. Insights on Beta-Hairpin Stability in Aqueous Solution from Peptides with Enforced Type I' and Type II' Beta-Turns. *J. Am. Chem. Soc.* **1997**, *119* (9), 2303–2304.
- (16) Lewandowska, A.; Oldziej, S.; Liwo, A.; Scheraga, H. A. Beta-Hairpin-Forming Peptides; Models of Early Stages of Protein Folding. *Biophys. Chem.* **2010**, *151* (1–2), 1–9.
- (17) Du, D.; Zhu, Y.; Huang, C. Y.; Gai, F. Understanding the Key Factors That Control the Rate of Beta-Hairpin Folding. *Proc. Natl. Acad. Sci. U.S.A.* **2004**, *101* (45), 15915–15920.
- (18) Brooks, C. L., 3rd. Protein and Peptide Folding Explored with Molecular Simulations. *Acc. Chem. Res.* **2002**, *35* (6), 447–454.
- (19) Ferrara, P.; Apostolakis, J.; Caflisch, A. Thermodynamics and Kinetics of Folding of Two Model Peptides Investigated by Molecular Dynamics Simulations. *J. Phys. Chem. B* **2000**, *104* (20), 5000–5010.
- (20) Chowdhury, S.; Zhang, W.; Wu, C.; Xiong, G. M.; Duan, Y. Breaking Non-Native Hydrophobic Clusters Is the Rate-Limiting Step in the Folding of an Alanine-Based Peptide. *Biopolymers* **2003**, *68* (1), 63–75.
- (21) Gnanakaran, S.; Nymeyer, H.; Portman, J.; Sanbonmatsu, K. Y.; Garcia, A. E. Peptide Folding Simulations. *Curr. Opin. Struct. Biol.* **2003**, *13* (2), 168–174.
- (22) Garcia, A. E.; Sanbonmatsu, K. Y. Alpha-Helical Stabilization by Side Chain Shielding of Backbone Hydrogen Bonds. *Proc. Natl. Acad. Sci. U.S.A.* **2002**, *99* (5), 2782–2787.
- (23) Sorin, E. J.; Pande, V. S. Exploring the Helix-Coil Transition Via All-Atom Equilibrium Ensemble Simulations. *Biophys. J.* **2005**, *88* (4), 2472–2493.
- (24) Buchete, N. V.; Hummer, G. Coarse Master Equations for Peptide Folding Dynamics. *J. Phys. Chem. B* **2008**, *112* (19), 6057–6069.
- (25) Kuczera, K.; Jas, G. S.; Elber, R. Kinetics of Helix Unfolding: Molecular Dynamics Simulations with Milestoning. *J. Phys. Chem. A* **2009**, *113* (26), 7461–7473.
- (26) Jas, G. S.; Kuczera, K. Computer Simulations of Helix Folding in Homo- and Heteropeptides. *Mol. Simulat.* **2012**, *38* (8–9), 682–694.
- (27) (a) Dinner, A. R.; Lazaridis, T.; Karplus, M. Understanding Beta-Hairpin Formation. *Proc. Natl. Acad. Sci. U.S.A.* **1999**, *96* (16), 9068–9073. (b) Klimov, D. K.; Thirumalai, D. Mechanisms and Kinetics of Beta-Hairpin Formation. *Proc. Natl. Acad. Sci. U.S.A.* **2000**, *97* (6), 2544–2549.
- (28) (a) Garcia, A. E.; Sanbonmatsu, K. Y. Exploring the Energy Landscape of a Beta Hairpin in Explicit Solvent. *Proteins: Struct., Funct., Genet.* **2001**, *42* (3), 345–354. (b) Zhou, R. H.; Berne, B. J.; Germain,

- R. The Free Energy Landscape for Beta Hairpin Folding in Explicit Water. *Proc. Natl. Acad. Sci. U.S.A.* **2001**, *98* (26), 14931–14936.
- (29) (a) Zagrovic, B.; Sorin, E. J.; Pande, V. Beta-Hairpin Folding Simulations in Atomistic Detail Using an Implicit Solvent Model. *J. Mol. Biol.* **2001**, *313* (1), 151–169. (b) Bolhuis, P. G. Transition-Path Sampling of Beta-Hairpin Folding. *Proc. Natl. Acad. Sci. U.S.A.* **2003**, *100* (21), 12129–12134.
- (30) Lwin, T. Z.; Luo, R. Force Field Influences in Beta-Hairpin Folding Simulations. *Protein Sci.* **2006**, *15* (11), 2642–2655.
- (31) Wei, G. H.; Mousseau, N.; Derreumaux, P. Complex Folding Pathways in a Simple Beta-Hairpin. *Proteins: Struct., Funct., Bioinf.* **2004**, *56* (3), 464–474.
- (32) (a) Thukral, L.; Daidone, I.; Smith, J. C. Structured Pathway across the Transition State for Peptide Folding Revealed by Molecular Dynamics Simulations. *PLoS Comput. Biol.* **2011**, *7* (9), e1002137. (b) Best, R. B.; Mittal, J. Microscopic Events in Beta-Hairpin Folding from Alternative Unfolded Ensembles. *Proc. Natl. Acad. Sci. U.S.A.* **2011**, *108* (27), 11087–11092. (c) De Sancho, D.; Mittal, J.; Best, R. B. Folding Kinetics and Unfolded State Dynamics of the Gb1 Hairpin from Molecular Simulation. *J. Chem. Theory Comput.* **2013**, *9* (3), 1743–1753.
- (33) (a) Marqusee, S.; Robbins, V. H.; Baldwin, R. L. Unusually Stable Helix Formation in Short Alanine-Based Peptides. *Proc. Natl. Acad. Sci. U.S.A.* **1989**, *86* (14), 5286–5290. (b) Munoz, V.; Serrano, L. Helix Design, Prediction and Stability. *Curr. Opin. Biotechnol.* **1995**, *6* (4), 382–386.
- (34) Shinitzky, M.; Goldman, R. Fluorometric Detection of Histidine-Tryptophan Complexes in Peptides and Proteins. *Eur. J. Biochem.* **1967**, *3* (2), 139–144.
- (35) Blanco, F. J.; Rivas, G.; Serrano, L. A Short Linear Peptide That Folds into a Native Stable Beta-Hairpin in Aqueous Solution. *Nat. Struct. Biol.* **1994**, *1* (9), 584–590.
- (36) Overton, M. C.; Blumer, K. J. Use of Fluorescence Resonance Energy Transfer to Analyze Oligomerization of G-Protein-Coupled Receptors Expressed in Yeast. *Methods* **2002**, *27* (4), 324–332.
- (37) Kirchhoff, W. H. *Exam (Coden: Ntnoef)*. U.S. Government Printing Office: Washington, DC, 1993; Vol. 1401.
- (38) (a) Dunn, B. M.; Pham, C.; Raney, L.; Abayasekara, D.; Gillespie, W.; Hsu, A. Interaction of Alpha-Dansylated Peptide Inhibitors with Porcine Pepsin - Detection of Complex-Formation by Fluorescence Energy-Transfer and Chromatography and Evidence for a 2-Step Binding Scheme. *Biochemistry* **1981**, *20* (25), 7206–7211. (b) Gustiananda, M.; Liggins, J. R.; Cummins, P. L.; Gready, J. E. Conformation of Prion Protein Repeat Peptides Probed by Fret Measurements and Molecular Dynamics Simulations. *Biophys. J.* **2004**, *86* (4), 2467–2483. (c) Bettio, A.; Dinger, M. C.; Beck-Sickinger, A. G. The Neuropeptide Y Monomer in Solution Is Not Folded in the Pancreatic-Polypeptide Fold. *Protein Sci.* **2002**, *11* (7), 1834–1844.
- (39) Brooks, B. R.; Brooks, C. L.; Mackerell, A. D.; et al. CHARMM: The Biomolecular Simulation Program. *J. Comput. Chem.* **2009**, *30* (10), 1545–1614.
- (40) Hess, B.; Kutzner, C.; van der Spoel, D.; Lindahl, E. GROMACS 4: Algorithms for Highly Efficient, Load-Balanced, and Scalable Molecular Simulation. *J. Chem. Theory Comput.* **2008**, *4* (3), 435–447.
- (41) Jorgensen, W. L.; Chandrasekhar, J.; Madura, J. D.; Impey, R. W.; Klein, M. L. Comparison of Simple Potential Functions for Simulating Liquid Water. *J. Chem. Phys.* **1983**, *79* (2), 926–935.
- (42) Duan, Y.; Wu, C.; Chowdhury, S.; et al. A Point-Charge Force Field for Molecular Mechanics Simulations of Proteins Based on Condensed-Phase Quantum Mechanical Calculations. *J. Comput. Chem.* **2003**, *24* (16), 1999–2012.
- (43) Kaminski, G. A.; Friesner, R. A.; Tirado-Rives, J.; Jorgensen, W. L. Evaluation and Reparametrization of the OPLS-AA Force Field for Proteins Via Comparison with Accurate Quantum Chemical Calculations on Peptides. *J. Phys. Chem. B* **2001**, *105* (28), 6474–6487.
- (44) (a) Matthes, D.; de Groot, B. L. Secondary Structure Propensities in Peptide Folding Simulations: A Systematic Comparison of Molecular Mechanics Interaction Schemes. *Biophys. J.* **2009**, *97* (2), 599–608. (b) Freddolino, P. L.; Liu, F.; Gruebele, M.; Schulter, K. Ten-Microsecond Molecular Dynamics Simulation of a Fast-Folding Ww Domain. *Biophys. J.* **2008**, *94* (10), L75–L77.
- (45) Frishman, D.; Argos, P. Knowledge-Based Protein Secondary Structure Assignment. *Proteins: Struct., Funct., Genet.* **1995**, *23* (4), 566–579.
- (46) Lednev, I. K.; Karnoup, A. S.; Sparrow, M. C.; Asher, S. A. Alpha-Helix Peptide Folding and Unfolding Activation Barriers: A Nanosecond UV Resonance Raman Study. *J. Am. Chem. Soc.* **1999**, *121* (35), 8074–8086.
- (47) Kabsch, W.; Sander, C. Dictionary of Protein Secondary Structure - Pattern-Recognition of Hydrogen-Bonded and Geometrical Features. *Biopolymers* **1983**, *22* (12), 2577–2637.
- (48) Pande, V. S.; Rokhsar, D. S. Molecular Dynamics Simulations of Unfolding and Refolding of a Beta-Hairpin Fragment of Protein G. *Proc. Natl. Acad. Sci. U.S.A.* **1999**, *96* (16), 9062–9067.
- (49) Best, R. B.; Mittal, J. Free-Energy Landscape of the GB1 Hairpin in All-Atom Explicit Solvent Simulations with Different Force Fields: Similarities and Differences. *Proteins* **2011**, *79* (4), 1318–1328.
- (50) Skwierawska, A.; Oldziej, S.; Liwo, A.; Scheraga, H. A. Conformational Studies of the C-Terminal 16-Amino-Acid-Residue Fragment of the B3 Domain of the Immunoglobulin Binding Protein G from Streptococcus. *Biopolymers* **2009**, *91* (1), 37–51.
- (51) Piana, S.; Lindorff-Larsen, K.; Shaw, D. E. How Robust Are Protein Folding Simulations with Respect to Force Field Parameterization? *Biophys. J.* **2011**, *100* (9), L47–L49.